Photoinduced absolute negative current in a symmetric molecular electronic bridge

Alexander Prociuk and Barry D. Dunietz
Department of Chemistry, The University of Michigan, Ann Arbor, Michigan 48109, USA
(Received 10 August 2010; revised manuscript received 26 August 2010; published 28 September 2010)

The study of current induced by photoradiating a molecular-based device under bias is of fundamental importance to the improvement of photoconductors and photovoltaics. In this technology, electron pumps generate an uphill current that opposes a potential drop and thereby recharges a fuel cell. While the modeled molecular electron pump is completely symmetric, the sign of the photocurrent is solely determined by the existing bias and the nature of photoinduced electronic excitations. The photoradiation induces nonequilibrium population of the electrode-coupled system. The dependence of the photocurrent on electrode coupling, photoradiation field strength, and applied bias are studied at a basic model level.

DOI: 10.1103/PhysRevB.82.125449 PACS number(s): 85.65.+h, 05.60.Gg, 72.40.+w, 73.63.−b

I. INTRODUCTION

Time-dependent (TD) electron transport through molecular and nanoscale systems will contribute an essential component to the development and function of future technology. The technological potential, along with a fundamental interest in the dynamics of molecular and nanoscale electronics,[1–3] motivates the large-scale research.[4–7] In particular, the use of solar radiation to control current flow through a molecular conductor provides an alternative to the difficult task of binding gating contacts within such spatially confined regions.[8–10] In general, TD fields can produce current flow between unbiased or even negatively biased electrodes by pumping electronic charge to excited states in a molecular photovoltaic or photoconductor, respectively.[5,11–17] Thus, under appropriate conditions, photoconductors can exhibit absolute negative conductance (ANC). Research efforts seek to exploit molecular properties to efficiently separate charge carriers using incident radiation.[18–20]

Here, we study photogenerated currents in a model molecular conducting bridge. The direction of the electronic current solely depends on the nature of the nonequilibrium population of the electronic pump state that follows photoexcitations. In the model only an applied potential bias introduces the required asymmetry. Additional structural asymmetries can be introduced to enhance the current pumping activity. Accurate computational models of molecular electron pumps must include the combined effect of bias, photoradiation, and molecule-electrode coupling on current. An understanding of these relations can then improve the ability of spectroscopy to study charge-transfer processes[21,22] and ultimately transform the pumping efficiency. We demonstrate that ANC can be achieved under proper photoexcitation of the molecule.

In general, molecular conductance is mediated by electronic states that are energy broadened upon electrode coupling. Electrons remain in wider broadened molecular states for shorter lifetimes before dispersing to the electrodes. On the other hand, stronger electrode coupling also reduces the electronic excitations' spectral cross section and therefore may reduce the photocurrent. We quantify photocurrent dependence on the involved electronic states' finite lifetimes to ultimately identify the conditions for optimal ANC. Recently, peaks and dips in the photocurrent energy distribution around the frequency of the oscillatory pumping field have been computationally modeled at the quantum dynamical level.[23] Photocurrent direction has also been shown to depend on the molecular system that coats an array of semiconducting nanoparticles.[24]

II. MODEL

The confined molecular pump is modeled by two states that are coupled strongly. The coupling is represented by β, an electronic interaction parameter, i.e., $H_{12}=H_{21}\equiv\beta$, where **H** is the electronic Hamiltonian. The resulting bonding and antibonding states are separated in energy by 2β. A third lower energy state ($H_{00}\equiv E_g$), that is also included in the model, is weakly coupled to these two states ($H_{02}=H_{20}=H_{01}=H_{10}\equiv\beta/50$). This energy level scheme is illustrated in Fig. 1, where the atomic-orbital (AO) representation is provided in part (a) and the corresponding molecular-orbital (MO) picture reflecting the coupling is given in part (b). The two strongly intercoupled orbitals are interfaced directly to electrodes resulting in a pair of conducting (broadened) states. In the AO representation this is achieved by coupling each site in the strongly interacting pair to its adjacent electrode by the parameter β_b. The coupling to the electrodes is represented by $\Sigma=\beta_b^{\dagger}g_s\beta_b$. In our model, the surface Green's function (GF) (g_s) is an imaginary constant number that implements a wide-band approximation for the electronic density of the electrode. The lowest state remains coupled (semibound) to the electrodes only through its weak interaction with the conducting states. The coupling effect broadens the MO energies and is illustrated in part (c). In part (d) we provide two electronic density of states (DOS) curves, where $\beta=-0.05$ (a.u.), $E_g=2\beta$. Each curve corresponds to a different band broadening with $\beta_b=0.2\beta$ and $\beta_b=\beta$.

In the two-level unbiased electrode-coupled subsystem, both the bonding and antibonding molecular orbitals are symmetrically distributed between the two atomic orbitals. The bias breaks this symmetry by polarizing the electronic states. For example, the projected electronic density of the bonding state on the site adjacent to the source electrode almost doubles in comparison to the projection on the site adjacent to the drain. This bias-induced polarization is re-

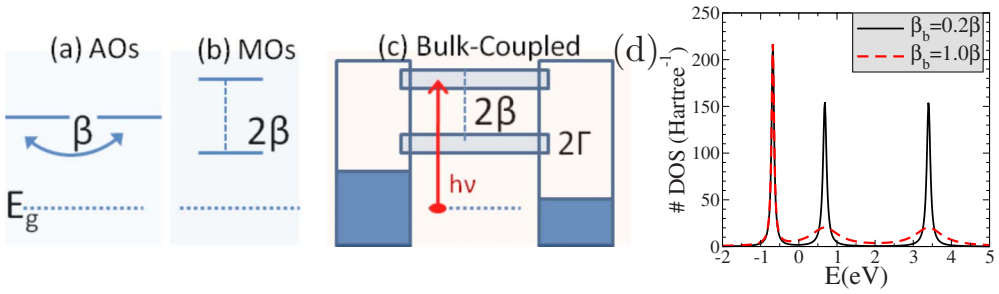

FIG. 1. (Color online) Schematic of the three-state system. (a) Localized/atomic-orbital representation, where the ground state E_g is weakly coupled (represented by dotted lines) to the conducting channels. The conducting states are coupled strongly to each other and to the leads. (b) Diagonalized molecular-orbital representation. (c) Broadened electronic density of states. Only the ground state is below the FE, which is set to zero. (d) The density of states of the confined system (see text for Hamiltonian definition).

versed for the antibonding state, an effect that leads to its stronger coupling with the drain upon bias. Positive photocurrent will therefore develop under nonequilibrium population of the excited broadened bonding orbital. Negative current, on the other hand, will develop upon population of the antibonding orbital (the higher excited state). To highlight this directed photoresponse we align (gate) the Fermi energy (FE) to lie between the ground state and the first conducting state and set it to zero without loss of generality. This FE alignment depletes both conducting orbitals at equilibrium. Organic conducting polymers of quinoidal derivatives exhibit related energetics, where planarity is enhanced due to the π bonding character of the excited state.[25]

The photocurrent is produced upon an applied TD potential: $\mathbf{v}(t)=\mathbf{v}_0+\mathbf{v}_{\mathrm{TD}}(t)$. The electronic excitations driving the photocurrent are induced by the radiation field that is represented by, $\mathbf{v}_{\mathrm{TD}}(t)$, an ac oscillatory pulse in the dipole approximation (i.e., in the AO representation $[\mathbf{v}_{\mathrm{TD}}(t)_{11}=-\mathbf{v}_{\mathrm{TD}}(t)_{22}=v_{\mathrm{TD}}(t)/2]$ and $[\mathbf{v}_{\mathrm{TD}}(t)_{01}=-\mathbf{v}_{\mathrm{TD}}(t)_{02}=0.05v_{\mathrm{TD}}(t)]$). The symmetry-breaking source-drain bias, $\mathbf{v}_0$, leading to the current direction is a steady ramping potential that is dropped across the system over the two electrode-coupled sites [in the AO representation: $(\mathbf{v}_0)_{11}=-(\mathbf{v}_0)_{22}=v_0/2$].

III. METHOD

Coupling to electrodes broadens the junction electronic DOS resulting in an energy redistribution of the electronic density matrix $[\rho(E)]$. Energy-broadened junction states may provide efficient transport channels. An operator's $(\hat{O})$ evolving expectation value can be obtained by tracing with the TD energy distribution of the electronic density $[\rho(E,t)]$,

$$\langle O(t)\rangle = \int dE\ \mathrm{Tr}[\rho(E,t)\hat{O}]. \tag{1}$$

We model the driven dynamical response of the system's electronic density using the Keldysh formalism. In this approach, electron dynamics is represented by the lesser GF, $G^<(x_1t_1,x_2t_2)$, that represents the solution to the electronic equation of motion (eom),

$$\left[i\frac{\partial}{\partial t}-h(xt)\right]G^<(xt,x't')=0, \tag{2}$$

$$[G^<(xt,x't')]^* = -G^<(x't',xt). \tag{3}$$

The variable x denotes a vector of the spatial coordinates. Localized basis functions are used to express the different operators. For example, the propagated $G^<$ is expressed in this localized AO basis as follows:

$$G^<(xt,x't')=\sum_{i,j}G^<_{i,j}(t,t')\phi_i(x)\phi_j(x') \tag{4}$$

and $h_{i,j}(t)=\int dx\phi_i(x)h(xt)\phi_j(x)$. In this representation we also write the overlap of the nonorthogonal basis functions as $S_{i,j}=\int dx\phi_i(x)\phi_j(x)$. The complete one-body Hamiltonian takes the following form:

$$\mathbf{h}(\mathbf{t})=\mathbf{h_0}+\mathbf{v}(\mathbf{t}), \tag{5}$$

where $\mathbf{h_0}\equiv\mathbf{H}$ as defined in the model description above. The system is propagated in an orthogonalized basis where $\mathbf{h}$ and $\mathbf{S}$ commute. Equations (2) and (3) become

$$\left[i\mathbf{1}\frac{\partial}{\partial t}-\mathbf{h}(t)\right]\mathbf{G}^<(t,t')=0, \tag{6}$$

$$[\mathbf{G}^<(t,t')]^\dagger=-\mathbf{G}^<(t',t). \tag{7}$$

Next, we combine these two equations and rewrite in terms of the time variables: $\bar{t}\equiv\frac{t_1+t_2}{2}$ and $\Delta t\equiv t_1-t_2$ to obtain

$$\frac{\partial}{\partial\bar{t}}\mathbf{G}^<(\bar{t},\Delta t)=i\left[\mathbf{G}^<(\bar{t},\Delta t)\mathbf{h}\left(\bar{t}-\frac{\Delta t}{2}\right)-\mathbf{h}\left(\bar{t}+\frac{\Delta t}{2}\right)\mathbf{G}^<(\bar{t},\Delta t)\right]. \tag{8}$$

The two time variable GF is the correlation function of an electronic system coupled to electron reservoirs as expressed on the Keldysh contour.[26,27] The dynamical electronic density $[\rho(E,t)$ in Eq. (1)] can be extracted from this GF by Fourier transforming from the Δt domain to the frequency $(\bar{\omega})$ or energy $(E=\hbar\bar{\omega})$ domain,[28]

$$\rho(E,\bar{t})=-i\int_{-\infty}^{\infty}d(\Delta t)e^{iE\Delta t}\mathbf{G}^<(\bar{t},\Delta t). \tag{9}$$

At steady state, the lesser GF describes the time-independent system as an energy distribution, where $G^<(t_1,t_2)\to G^<(t_1-t_2)$ and, therefore, $\rho(E,\bar{t})\to\rho(E)$.

We use the Fourier transform to express the lesser GF in a form appropriate for using TD perturbation theory (PT). First, the lesser GF is expressed in the mixed (time-frequency) representation of the perturbing potential $\mathbf{v}_{\mathrm{TD}}(t)$, which is defined as $\mathbf{v}(\bar{t},\bar{\omega}) \equiv \frac{1}{\pi} e^{-i2\bar{\omega}\bar{t}} \tilde{\mathbf{v}}(2\bar{\omega}) = \frac{1}{\pi} e^{-i2\bar{\omega}\bar{t}} \int_{-\infty}^{\infty} dt e^{i(2\bar{\omega})t} \mathbf{v}_{\mathrm{TD}}(t)$. Here, $\tilde{\mathbf{v}}(\omega)$ is the Fourier transform of the applied TD potential $\mathbf{v}_{\mathrm{TD}}(t)$. In this representation the $G^<$ electronic Kadanoff-Baym (K-B) eoms (Refs. 26 and 27) of the coupled open system take the following form:

$$i\frac{\partial}{\partial \bar{t}}\Delta\mathbf{G}^<(\bar{t},\bar{\omega}) = [\mathbf{h_0}+\mathbf{v_0},\Delta\mathbf{G}^<(\bar{t},\bar{\omega})] + \int d\omega'[\mathbf{v}(\bar{t},\omega')\mathbf{G}^<(\bar{t},\bar{\omega}-\omega') - \mathbf{G}^<(\bar{t},\bar{\omega}+\omega')\mathbf{v}(\bar{t},\omega')]$$
$$+ \int_{-\infty}^{\infty} dt'[\mathbf{\Sigma}^{\mathbf{R}}(\bar{t}-t')\Delta\mathbf{G}^<(t',\bar{\omega})e^{-i\mathbf{h_0}(\bar{t}-t')} - e^{i\mathbf{h_0}(\bar{t}-t')}\Delta\mathbf{G}^<(t',\bar{\omega})\mathbf{\Sigma}^{\mathbf{A}}(t'-\bar{t})], \tag{10}$$

where the Σ's as defined above project the infinite nature of the system to the bridge space and $\mathbf{v_0}$ is the bias.[28] Above, the $\Delta\mathbf{G}^<(\bar{t},\bar{\omega})$ is defined to be the difference between the total lesser GF, $\mathbf{G}^<(\bar{t},\bar{\omega})$, and the steady state lesser GF under applied constant bias is $\mathbf{G}^{0,<}_{v_0}(\bar{\omega})$, i.e., $\mathbf{G}^<(\bar{t},\bar{\omega}) \equiv \mathbf{G}^{0,<}_{v_0}(\bar{\omega}) + \Delta\mathbf{G}^<(\bar{t},\bar{\omega})$. In other words, the open system's electronic structure under the effect of $\mathbf{v}_0$ is used as the reference to the TD-PT and is represented by $\mathbf{v}_{\mathrm{TD}}(t)$.

The direct propagation of these eoms is computationally demanding mainly due to the self-energy memory-dependent terms in the expansion [see Eq. (10)]. We find that in the full frequency representation, where $G^<(\Delta\omega,\bar{\omega}) \equiv \int_{-\infty}^{\infty} d\bar{t} e^{i\Delta\omega\bar{t}} G^<(\bar{t},\bar{\omega})$, the application of the TD-PT treatment becomes more effective than in the mixed representation. In the PT expansion expressed in the frequency domain the bulk self-energies are written exactly; for example, without using the wide-band approximation. The eom takes the following form:[29]

$$\sum_{k,l} \mathcal{H}_{ijkl}(\Delta\omega)\Delta G^<_{kl}(\Delta\omega,\bar{\omega}) = B^{(1)}(\Delta\omega,\bar{\omega})_{ij} + \frac{1}{\pi}\int d\omega'[\tilde{\mathbf{v}}(2\omega')\Delta\mathbf{G}^<(\Delta\omega-2\omega',\bar{\omega}-\omega') - \Delta\mathbf{G}^<(\Delta\omega-2\omega',\bar{\omega}+\omega')\tilde{\mathbf{v}}(2\omega')]_{ij}, \tag{11}$$

where

$$\mathcal{H}_{ijkl}(\Delta\omega) \equiv (\Delta\omega + i\eta - \Delta\epsilon_{ij})\delta_{ik}\delta_{jl} - \Gamma_{ijkl}(\Delta\omega) - (\mathbf{v_0}_{ik}\delta_{lj} - \mathbf{v_0}_{lj}\delta_{ik}). \tag{12}$$

Here

$$\mathbf{B^{(1)}}(\Delta\omega,\bar{\omega}) \equiv [\tilde{\mathbf{v}}(\Delta\omega)\mathbf{G}^{0,<}_{v_0}(\bar{\omega}-\Delta\omega/2) - \mathbf{G}^{0,<}_{v_0}(\bar{\omega}+\Delta\omega/2)\tilde{\mathbf{v}}(\Delta\omega)] \tag{13}$$

and $\Gamma_{ijkl}(\Delta\omega)$ is the broadening function due to coupling to the electrodes that is generalized to include dynamical effects (memory kernel) by defining

$$\Gamma_{ijkl}(\Delta\omega) \equiv \int dt e^{i\Delta\omega t}\Gamma_{ijkl}(t) = \Sigma^R_{ik}(\epsilon_j+\Delta\omega)\delta_{lj} - \Sigma^A_{lj}(\epsilon_i-\Delta\omega)\delta_{ik}. \tag{14}$$

In the above equation $\Delta\epsilon_{ij} \equiv \epsilon_i - \epsilon_j$ is the difference between the ith and jth eigenvalues (ϵ_i,ϵ_j) of h_0. The bias $(\mathbf{v_0})$ effect is entered in the expansion treatment but also in defining the $\mathcal{H}$ superoperator. The implemented formalism includes a broadening factor (η).

This full frequency representation indeed lends itself to the use of TD-PT to solve for the response of the system, $\Delta G^<$, to the applied perturbation $v(t)$. Recently, we have solved this expansion of the K-B equations[26,27] to first order for model open systems under nonequilibrium conditions to analyze transient currents, spectra of biased systems, and transport driven by ac fields.[28–30] However, here we show that the second-order term of the PT expansion in the TD field $(\mathbf{v}_{\mathrm{TD}}(t))$ is required to model the driven current.

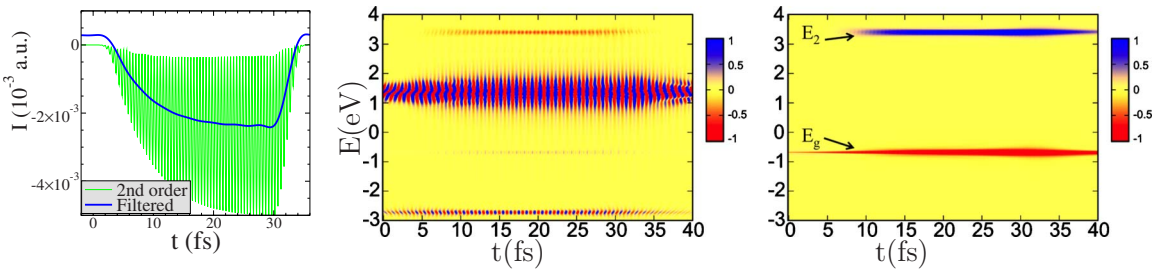

FIG. 2. (Color online) (Left) Total TD current (low-frequency filtered) and second-order contribution to the TD current. (Center) TD distribution of the current as illustrated with a color map. (Right) TD distribution of the population transferred during the course of the excitation (negative values indicate population loss) as illustrated with a color map. The band structure of the density operator involves a positive feature at the second excited state energy (E_2) and a negative feature at the ground-state energy (E_g).

In the final expression, which can be expanded to nth order in the perturbation, we express the TD electronic density in terms of the evolving occupations of the projected device states.[29] The band structure due to the coupling to the electrodes is included directly in this expansion through the energy distribution variable. We note that Eq. (11) involves a tensor of rank four that is traced with a matrix (tensor of rank 2).

At the steady state, any transient or TD aspects due to applied bias are completely dissipated. The steady-state description is achieved by a proper time-independent limit of the above treatment, where the corresponding time-independent perturbation $\mathbf{v}(t) \equiv \mathbf{v_0}$ is Fourier transformed as in Eq. (11) to the frequency domain,

$$\mathbf{v}(\Delta\omega) = 2\pi\delta(\Delta\omega)\mathbf{v_0}. \tag{15}$$

For the steady state, the two-frequency based representation of the eoms is collapsed to a single variable expansion. The resulting expression describes a time-independent correction to the unbiased system represented by $G^{0,<}$,

$$\mathbf{G}^{\mathbf{0},<}_{\mathbf{v_0}}(\bar{\omega})_{ij} = \mathbf{G}^{0,<}(\bar{\omega}) + \mathcal{H}^{-1}_{ijkl}(0)B^{(1)}_{v_0}(\bar{\omega})_{kl}. \tag{16}$$

In calculating $B^{(1)}_{v_0}(\bar{\omega}) \equiv \mathbf{v_0}\mathbf{G}^{0,<}(\bar{\omega}) - \mathbf{G}^{0,<}(\bar{\omega})\mathbf{v_0}$, we use the relationship between $\mathbf{G}^{<}(\bar{\omega})$ and the retarded GF, $\mathbf{G}^{R}(\bar{\omega})$, which entails calculating the Fermi matrix.[28]

IV. RESULTS AND DISCUSSION

First, we confirm that optical pumping of sufficient population into the excited antibonding orbital leads to ANC. The dc-biased model system (steady source drain bias v_0) is affected by an ac potential $[\mathbf{v}_{\mathrm{TD}}(t)]$ tuned to the excitation energy between the ground and the second excited states ($\nu \equiv \omega_0/(2\pi) = 4.1$ eV $\approx |E_g| + |\beta|$) with a 0.1 eV amplitude. The TD current is illustrated in the left panel of Fig. 2. The nonoscillatory component of the current is obtained by a low-pass filter and exhibits ANC. The contributions to the current resolved in the energy domain (energy distributions) are shown with the color map in the central panel. From this TD energy distribution, the TD current can be calculated by integrating over the energy at each time point. The evolving band structure of the current operator includes two major features. The first-order term in the PT expansion is the coherent response to the ac field that leads to symmetric (about zero) oscillations [not shown in the $I(t)$ curve] at the frequency that is equal to the transition energy. A resonant first-order band, that is the most dominant feature, is centered energetically midway between the interfering orbitals. An additional first-order miniband arising from the same interference is observed at a negative energy shift below the ground state.[28,29] A second-order weaker oscillatory band with twice the transition frequency is found at the ground-state energy and is reflected in the oscillating second-order curve (left panel).

Second-order terms are required to address the transfer of population that follows from the coherence. Indeed, an additional second-order nonoscillatory negative feature in the current's energy distribution is aligned with the highest excited state energy. The negative flow is therefore confirmed to emerge from the nonequilibrium population of the second excited orbital. The band structure of the density operator confirms this assignment (right panel). Direct positive current is contributed by the ground-state orbital and is expected to increase for higher biases or increased coupling of the ground state to the electrodes.

We use the dynamical treatment to analyze the complex interplay between electrode coupling, dc bias, and the resonant ac field. We compare the negative photocurrent component to the positive (steady-biased) dc under varied coupling-induced finite lifetimes of the ground state and the excited conducting states. We first consider the direct coupling of the ground state with the electrode ($H_{0,\mathrm{bulk}}$), which is varied from 0 to 0.2β. The resulting currents are provided in Fig. 3. The positive dc is enhanced with increased coupling as reflected by the black curve measured with the vertical axis on the right side of the plot. This positive current is mainly due to population of the first excited state upon applying the bias. The negative response due to the photocurrent curve is measured with the left vertical axis. This photocurrent is inversely related to the electrode coupling. We also compare the photoresponse under the effect of two fields (ac amplitudes of 0.04 and 0.1 eV). In the plot, the response curve for the lower field amplitude is scaled up by a factor of 5 that is close to the ratio between the two intensities, 25/4. The field intensities ratio determines the relationship between the respective photocurrents in the large conductance (i.e., strong electrode coupling) regime. For smaller values of electrode coupling, the ratio of the photocurrents exceeds the field in-

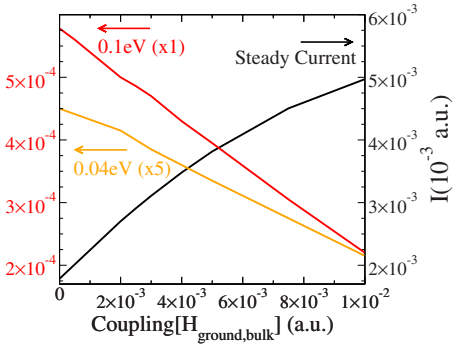

FIG. 3. (Color online) (Right axis) Current under 0.566 V ($=0.4\beta/e$) bias with a range of direct ground-state electrode couplings (H_{0L},H_{0R}). (Left axis) Magnitudes of negative currents induced by the radiation field. (The weaker field's response is scaled by a factor of 5.)

tensities fraction. We note that in these trends the total current remains positive.

We now consider the effect of the excited states' electrode coupling, that is parametrized by β_b with values that range from 0.1β to β. An increased β_b enhances the tunneling resonance between the excited state and the source electrode. However, the dissipative coupling leads to a reduction of the spectral peak associated with the optical excitations. In Fig. 4, we plot low-pass filtered TD currents under a range of junction-electrode coupling strengths ($H_{1,\text{bulk}}=H_{2,\text{bulk}}\equiv\beta_b$). A source-drain bias of 0.136 V (i.e., a bias of $0.1\beta/e$, where e is the fundamental unit of charge) and an ac field of 0.1 eV amplitude are applied to this system. We see in Fig. 4 that an increase in the orbital's conductance results in an expected increase in the positive dc current and a reduction in the photoresponse. As shown in the plot a sufficiently small coupling value results in ANC.

The corresponding ratio between the negative photocurrent and the steady current under the scanned device-bulk coupling strengths is shown for steady biases of 0.136 and 0.544 V ($0.1\beta/e$ and $0.4\beta/e$). For both biases the ratio exceeds 1 at sufficiently weak electrode coupling leading to ANC. The photoinduced ANC becomes dominant only under a further weakening of the coupling to the electrodes. Namely, ANC develops at conditions whereby the cross section for the electronic excitation is sufficiently large in comparison to the dissipative broadening due to electrode coupling. We also emphasize that increasing the voltage bias reduces the relative weight of the photocurrent to the total current. Namely, the dissipative effect of electrode coupling, responsible for the reduction in the spectral cross section, dominates over its ability to enhance the photocurrent when a bias is applied.

V. CONCLUDING REMARKS

Transport through open quantum systems follows from phase coherence between the charge carriers and the electrodes. The ability to manipulate these coherences by photoexcitation is used to pump electronic charge through a symmetric model molecular system. In the model, two electrode-contacted sites are mutually coupled resulting in a bonding and antibonding orbital pair. An ANC will develop upon photoinduced nonequilibrium population of the higher antibonding orbital that features a stronger coupling with the source electrode upon a steady bias. We use a TD approach to analyze the photocurrent dependence on electrode coupling strengths of the electronic states that are coupled by the radiation field. We solve the electronic equations of motion as expressed within the Keldysh formalism using nonequilibrium Green's function. The calculations employ a TD-PT expansion, where second-order terms determine the ANC.

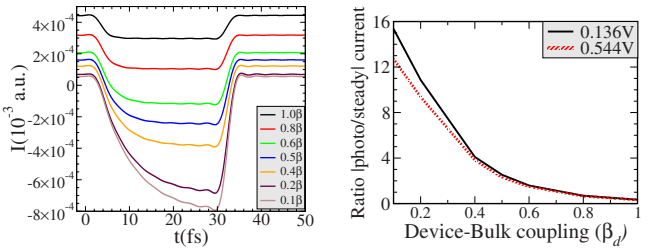

FIG. 4. (Color online) (Left) The TD directed current under different electrode-device coupling strengths ($H_{b,i}$). (Right) The corresponding ratio between the negative induced current and the steady dc flux. (Absolute negative current is effected at ratios larger than 1.)

We find that the photocurrent contribution to the total current is mainly determined by the electronic excitation cross section. The excitation cross section decreases with stronger coupling of either the ground or excited states to the electrodes. Therefore, the ratio of photocurrent to total current reduces with stronger coupling of the bridge states with the electrodes. This is in spite of the prospect that stronger conductance properties of the related excited state would increase the overall photocurrent. This is an important result that will assist efforts to enhance ANC, for example, by introducing structural asymmetries. We emphasize that these relationships are general and are expected to prevail for electron transport through molecules attached to electrodes and through bulk-coupled quantum dots under microwave radiation.

ACKNOWLEDGMENTS

B.D.D. is supported as part of the Center for Solar and Thermal Energy Conversion, an Energy Frontier Research Center funded by the U.S. Department of Energy, Office of Science, Office of Basic Energy Sciences under Award No. DE-SC0000957. B.D.D. and A.P. thank Heidi Phillips and Shaohui Zheng for assistance in figure preparation.

[1] A. Nitzan and M. A. Ratner, Science **300**, 1384 (2003).
[2] J. Kushmerick, J. Lazorcik, C. Patterson, R. Shashidhar, D. Seferos, and G. Bazan, Nano Lett. **4**, 639 (2004).
[3] F. Chen, J. Hihath, Z. Huang, X. Li, and N. J. Tao, Annu. Rev. Phys. Chem. **58**, 535 (2007).
[4] L. P. Kouwenhoven, A. T. Johnson, N. C. van der Vaart, C. J. P. M. Harmans, and C. T. Foxon, Phys. Rev. Lett. **67**, 1626 (1991).
[5] M. Switkes, C. M. Marcus, K. Campman, and A. C. Gossard, Science **283**, 1905 (1999).
[6] P. J. Leek, M. R. Buitelaar, V. I. Talyanskii, C. G. Smith, D. Anderson, G. A. C. Jones, J. Wei, and D. H. Cobden, Phys. Rev. Lett. **95**, 256802 (2005).
[7] Z. Zhong, N. M. Gabor, J. E. Sharping, A. L. Gaeta, and P. L. MCeuen, Nat. Nanotechnol. **3**, 201 (2008).
[8] J. Lehmann, S. Kohler, P. Hänggi, and A. Nitzan, Phys. Rev. Lett. **88**, 228305 (2002).
[9] S. Kohler, S. Camalet, M. Strass, J. Lehmann, G.-L. Ingold, and P. Hanggi, Chem. Phys. **296**, 243 (2004).
[10] V. May and O. Kühn, Phys. Rev. B **77**, 115440 (2008).
[11] L. P. Kouwenhoven, S. Jauhar, J. Orenstein, P. L. McEuen, Y. Nagamune, J. Motohisa, and H. Sakaki, Phys. Rev. Lett. **73**, 3443 (1994).
[12] N. C. van der Vaart, S. F. Godijn, Y. V. Nazarov, C. J. P. M. Harmans, J. E. Mooij, L. W. Molenkamp, and C. T. Foxon, Phys. Rev. Lett. **74**, 4702 (1995).
[13] T. H. Oosterkamp, T. Fujisawa, W. G. van der Wiel, K. Ishibashi, R. V. Hijman, S. Tarucha, and L. P. Kouwenhoven, Nature (London) **395**, 873 (1998).
[14] F. Zhou, B. Spivak, and B. Altshuler, Phys. Rev. Lett. **82**, 608 (1999).
[15] S. Kohler, J. Lehmann, and P. Hanggi, Phys. Rep. **406**, 379 (2005).
[16] M. D. Blumenthal, B. Kaestner, L. Li, S. Giblin, T. J. B. M. Janssen, M. Pepper, D. Anderson, G. Jones, and D. A. Ritchie, Nat. Phys. **3**, 343 (2007).
[17] B. Kaestner *et al.*, Phys. Rev. B **77**, 153301 (2008).
[18] B. O'regan and M. Grätzel, Nature (London) **353**, 737 (1991).
[19] H. J. Snaith and M. Grätzel, Phys. Rev. Lett. **98**, 177402 (2007).
[20] O. V. Prezhdo, W. R. Duncan, and V. V. Prezhdo, Prog. Surf. Sci. **84**, 30 (2009).
[21] A. C. Morteani, P. Sreearunothai, L. M. Herz, R. H. Friend, and C. Silva, Phys. Rev. Lett. **92**, 247402 (2004).
[22] S. Sulaiman, A. Bhaskar, J. Zhang, R. Guda, T. Goodson III, and R. M. Laine, Chem. Mater. **20**, 5563 (2008).
[23] N. Tsuji, T. Oka, and H. Aoki, Phys. Rev. Lett. **103**, 047403 (2009).
[24] H. Nakanishi, K. J. M. Bishop, B. Kowalczyk, A. Nitzan, E. A. Weiss, K. V. Tretiakov, M. M. Apodaca, R. Klajn, J. F. Stoddart, and B. A. Grzybowski, Nature (London) **460**, 371 (2009).
[25] R. S. Becker, J. Sexias de Melo, A. L. Macanita, and F. Elisei, J. Phys. Chem. **100**, 18683 (1996).
[26] L. P. Kadanoff and G. Baym, *Quantum Statistical Mechanics* (Benjamin and Cummings, New York, 1962).
[27] M. Bonitz, *Quantum Kinetic Theory* (Teubner, Stuttgart, 1998).
[28] A. Prociuk and B. D. Dunietz, Phys. Rev. B **78**, 165112 (2008).
[29] A. Prociuk, H. Phillips, and B. D. Dunietz, J. Phys.: Conf. Ser. **220**, 012008 (2010).
[30] A. Prociuk and B. D. Dunietz, *Atomic and Molecular Systems, Dynamics, Spectroscopy, Clusters, and Nanostructures*, Progress in Theoretical Chemistry and Physics Vol. 20 (Springer, Netherlands, 2009), pp. 265–277.